Regular paper

Implementation and experimental verifications of microstrip antennas for angular scanning of a Doppler radar

Anıl Karatay, Durmuş Orcan, Ceren Özkal, Fatih Yaman *

Department of Electrical & Electronics Engineering, Izmir Institute of Technology, Izmir, Turkey

ARTICLE INFO

ABSTRACT

The aim of this study is to improve operational capabilities and range of the MIT-Coffee Can Doppler radar via aperture coupled Vivaldi type transmitter antenna, patch array receiver antenna, and an unequal power divider. Accordingly, a mechanical angular scanning feature for tracking multi-targets and the system integration of lightweight microstrip structures are realized for the radar. A narrow beamwidth in the receiver and a well impedance matching on the overall system to reduce return losses are achieved for the considered application. Good agreements between simulations and measurements for the fabricated antennas/divider and a successful integration of the antennas to the existing system for finding a moving target angular location is reported. It is shown that through wall identification and target velocity at scanned regions can be obtained with the proposed hardware configuration. Simulation results of antenna parameters for various number of array elements are listed which could be a useful tool for different engineering applications.

1. Introduction

Doppler radars are used to determine velocity of moving objects from the frequency shifts of transmitted and received electromagnetic waves. They are employed for vital signal detection [1,2], signature extraction from ballistic target in military applications [3], Doppler navigation [4], monitoring vibrations and long term motions of civil structures [5], identifying atmospheric changes in weather forecast studies [6], and detection of rotating or moving bodies in astronomy [7]. In this context, MIT-Coffee Can type Doppler radar operates at 2.45 GHz to detect ranges and velocities of moving targets having relatively low speeds in relatively short ranges which are reported in numerous studies [8–16]. In this study, existing radar is converted to a portable form by replacing cantennas with microstrip antennas. In addition, a new mechanical angular scanning capability is integrated to the system using a pencil beam array antenna. Furthermore, the range of the radar is increased by a splitter exploiting unequal power division. Having done those improvements in the system, the applicability and efficiency for line-of-sight and through wall scenarios are experimentally investigated.

Recently, Gennarelli et al. [17] presented detections of objects behind the wall via employing a radar system with horn antennas.

However, to achieve through wall identifications with low-cost and lightweight antennas, which will be addressed in this study, is an advantage from practical point of view. Furthermore, angular information of the targets located behind a concrete wall is provided. The manuscript expresses range data for different scenarios and radar performance comparisons for different antenna mountings in terms of footprint, back-lobe level, weight and mutual coupling.

There is a wide range of information available for Doppler radars in the open literature however we can cover only few of references in here, see [8–30]. The mentioned studies present general context on the principles of Doppler radars, measurement results and different designs for transmitter and receiver antennas. Among them, the papers [8,9] present basics and block diagrams of Doppler radars operating at 2.4 GHz and at 6 GHz, respectively. Furthermore, the books [18–20] provide fundamental formulations for design parameters of radar components and their limitations.

In this work, the receiver antenna of the Doppler radar is considered as a microstrip four-element array which is originated from the studies [21–25]. However, while the paper [21] is focused on a single patch antenna the proposed designs are modified and optimized according to the chosen application needs. In particular, the number of array elements is increased to achieve the desired pencil beam for angular scanning and far-field gain is maximized for a larger radar range at 2.45 GHz. The papers [26–29] describing microstrip-fed Vivaldi antennas are used to guide the design study

---

* Corresponding author.
  E-mail address: fatihyaman@iyte.edu.tr (F. Yaman).

of the transmitter antenna. For instance, possible far-field results of the transmitter in elevation plane and feeding methods of Vivaldi antennas are investigated in [27], formulations on the exponential shape of the ground plane and the input impedance of the feed-line of an antenna for an antipodal Vivaldi antenna are derived in [28] and a relationship between operating frequency, dielectric constant, conductor width and flare width for an antipodal Vivaldi antenna is adapted to a microstrip-fed aperture coupled Vivaldi antenna for a certain frequency in [29].

The organization of the paper is as follows. The next two sections are devoted to explain details of the optimum design parameters obtained from CST simulations for the receiver (Rx) and transmitter antennas (Tx). In Section 4 simulation and measurement results are compared for S-parameters and radiation patterns of the antennas. The following section focuses on reporting experimental results obtained by the radar with newly designed microstrip antennas and angular scanning feature. Final remarks, observations and experiences are discussed in the conclusions section. In the Appendix A, far field gain patterns in polar form, main, side lobe magnitude levels, 3 dB beamwidth and the width of array antennas for different number of elements are presented.
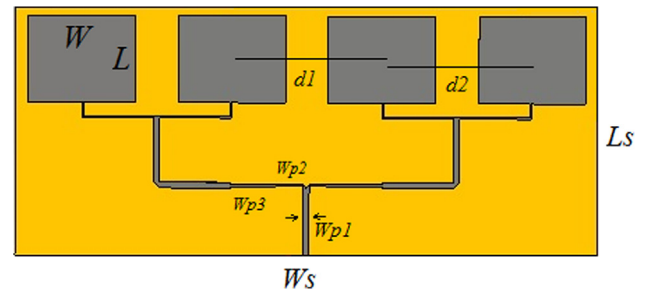
2. Receiver antenna design

In principle, width (W) and length (L) of a single element patch antenna can be calculated for a given operating frequency (f_0), relative dielectric permittivity of the substrate material (ε_r), and substrate height (h) via well-known microstrip antenna formulas, see [19–21]. Even though further detailed investigations on single/-multi element(s) patch antennas can be found in [31,32] the parametric sweep studies via 3-D full Maxwell system solvers are needed for determining complete electromagnetic behaviour of the initial design and achieving application requirements on beamwidth, gain, directivity, etc. In this context, observations and results from the numerical experiments on the final antenna design parameters are discussed in the following.

One can obtain narrower 3-dB beamwidth and larger main/side lobe magnitudes by increasing the number of elements in the array antenna design according to the simulation results given in Appendix A. This result brings a trade-off between the number of elements in the array antenna and the compactness of the structure. Therefore, 4×1 array antenna has been chosen as an optimal design according to the needs of mechanical angular scanning. FR-4 with thickness 1.5 mm is chosen as a substrate material for the receiver antenna due to its easy access. Slight increases in the magnitude of the main/side lobes could be achieved for the smaller permittivity. Nevertheless, since the half power beam width increases for the larger dielectric constant values, FR-4 remains a reasonable choice for the prototype. Thickness of the substrate does not cause any significant change in 3-dB beamwidth but rise in the height of the substrate increases both main and side lobe magnitudes [31].

Table 1 presents the final dimensions for the receiver under the guidance of mentioned simulation results with acceptable gain and main/side lobe levels (see Fig. 1).

Fig. 1. Microstrip antenna design with 4 elements.

3. Transmitter antenna design

The Vivaldi antenna is designed as the transmitter antenna of the radar thanks to its small physical dimensions, wide bandwidth and desired directivity property. Furthermore, unlike the receiver, the transmitter antenna does not need to have pencil beam characteristics or a low back lobe magnitude. In fact, if the transmitter antenna had a lower 3-dB beamwidth, some objects could be missed during angular scanning due to the distance between antennas. The final design parameters obtained for the transmitter antenna are given in Table 2. Among them, the geometry related ones are indicated in Fig. 2.

In Table 2, h represents the thickness of the substrate, ε_r is the relative dielectric constant of the substrate, ε_e is the effective dielectric constant.

The impedance matching between the feed line of the antenna and the connector, and also the operating frequency of the antenna can be found via standard Vivaldi antenna formulas, see [26–29].

4. Simulation and measurement results for antennas

This section is devoted to the verifications of the antenna simulations with the measurements. Moreover, 3-D radiation patterns and power flows of transmitter and the receiver antennas are illustrated.

In Fig. 3 return loss of the antennas are presented. Simulations are prepared with CST-MWS frequency domain solver whereas the measurements are done using a Vector Network Analyser (VNA). As can be seen in Fig. 3, both antennas have the scattering matrix element S_{11}, below 30 dB which indicates a good impedance match to a 50 Ω coaxial cable at 2.45 GHz. The measurement and simulation results for S_{11} match more accurately for the transmitter antenna as compare to the receiver antenna. The reason is mostly a poor resolution for realizing thin microstrip lines existing on the array antenna in the manufacturing technique.

However, such a discrepancy helped us to reach a better power transfer capability for the receiver antenna for instance approximately 99% of the received power can be transferred to the mixer. This value is slightly higher for the transmitter antenna e.g. Vivaldi antenna can transmit 99.906% of the incident signal to the free space at 2.45 GHz. These results assure that both antennas are proper for the radar application.

Table 1
Dimensions for the receiver antenna with 4 elements.

Parameter	Value (mm)	Parameter	Value (mm)
h	1.5	W	36.2
L	28.1	Ws	220
Ls	100	Wp1	2.93
d1	50	Wp2	0.73
d2	49	Wp3	1.69

Table 2
Design parameters of the Vivaldi antenna.

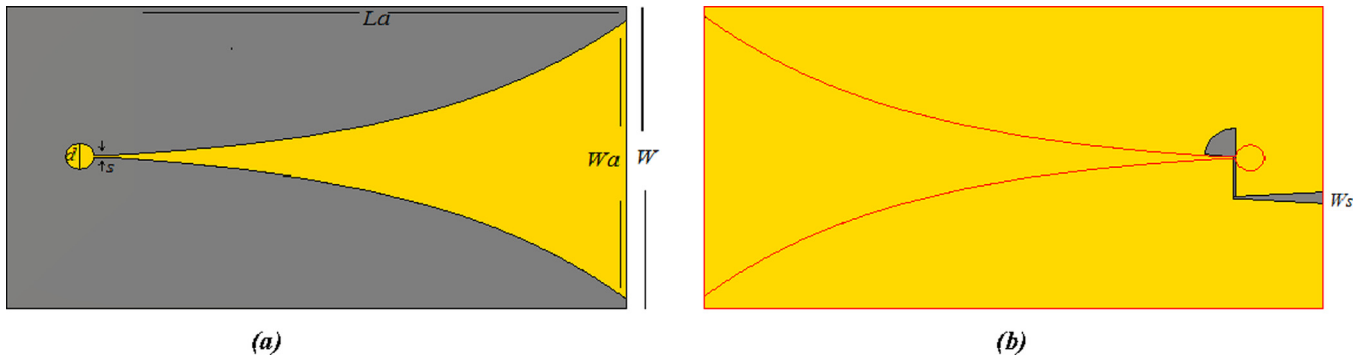| Parameter	Value & Unit	Parameter	Value & Unit
ε_r	4.3 (unitless)	L_a	101.48 mm
ε_e	3.26 (unitless)	W_s	2.44 mm
s	0.50 mm	f	2.45 GHz
W_a	60.70 mm	W	65.75 mm
d	5.69 mm	h	1.50 mm

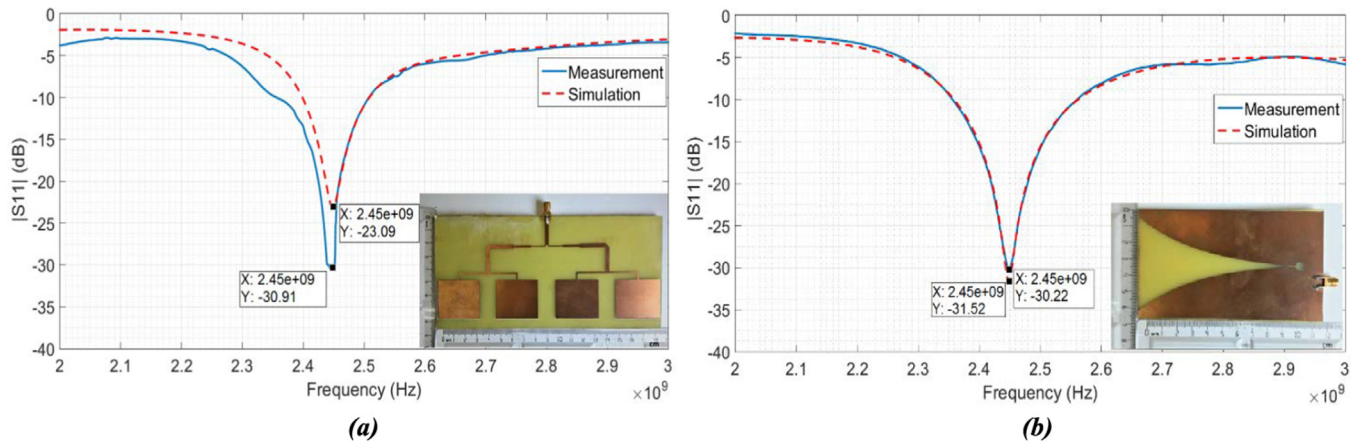**Fig. 2.** Tx Vivaldi antenna. (a) Ground plane. (b) Feedline.

Fig. 3. Simulation and measurement of S_{11} results of the antennas. (a) S_{11} of Rx array antenna (b) S_{11} of Tx Vivaldi antenna.

Far-field patterns shown in Fig. 4 are measured with gain transfer method in the anechoic chamber at IZTECH. A wideband and the directive horn antenna operating at 2–18 GHz frequency range is used as a transmitter with 25 dBm output power. The discrete appearance of the measurement curves in Fig. 4 is related to the limited amount of the data was collected with a step size of 9 degrees for Vivaldi and of 10 degrees for array antenna due to some mechanical limitations in the rotating system. Nevertheless, the measurements gave us sufficient information about the pattern of the antennas and agreed well the simulation results.

As a last step before the system integration, 3-D gain patterns and power flow distributions of the both antennas are simulated using CST-MWS, which are shown in linear and logarithmic scales in Fig. 5, respectively. Among those results, the 3-D radiation patterns help to determine the correct angular mounting orientations of each antenna for sweeping the desired sections in the radar range. Furthermore, maximum gain of the pencil beam array can be read as ~1.75 times larger than the Vivaldi antenna from Fig. 5a and b. This can be explained by observing the fine power flow of the array antenna as compare to Vivaldi illustrated in Fig. 5c and d. It can be
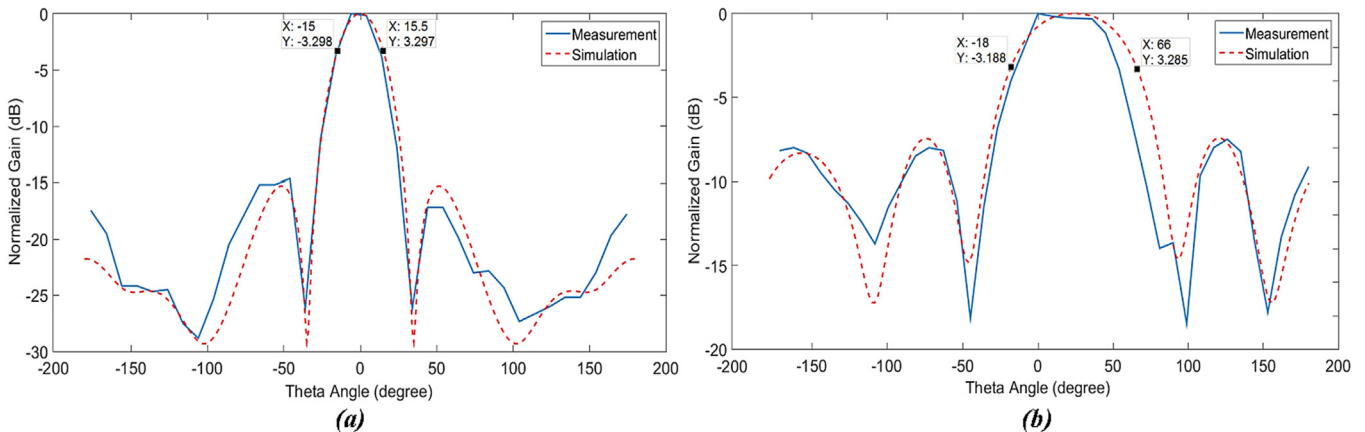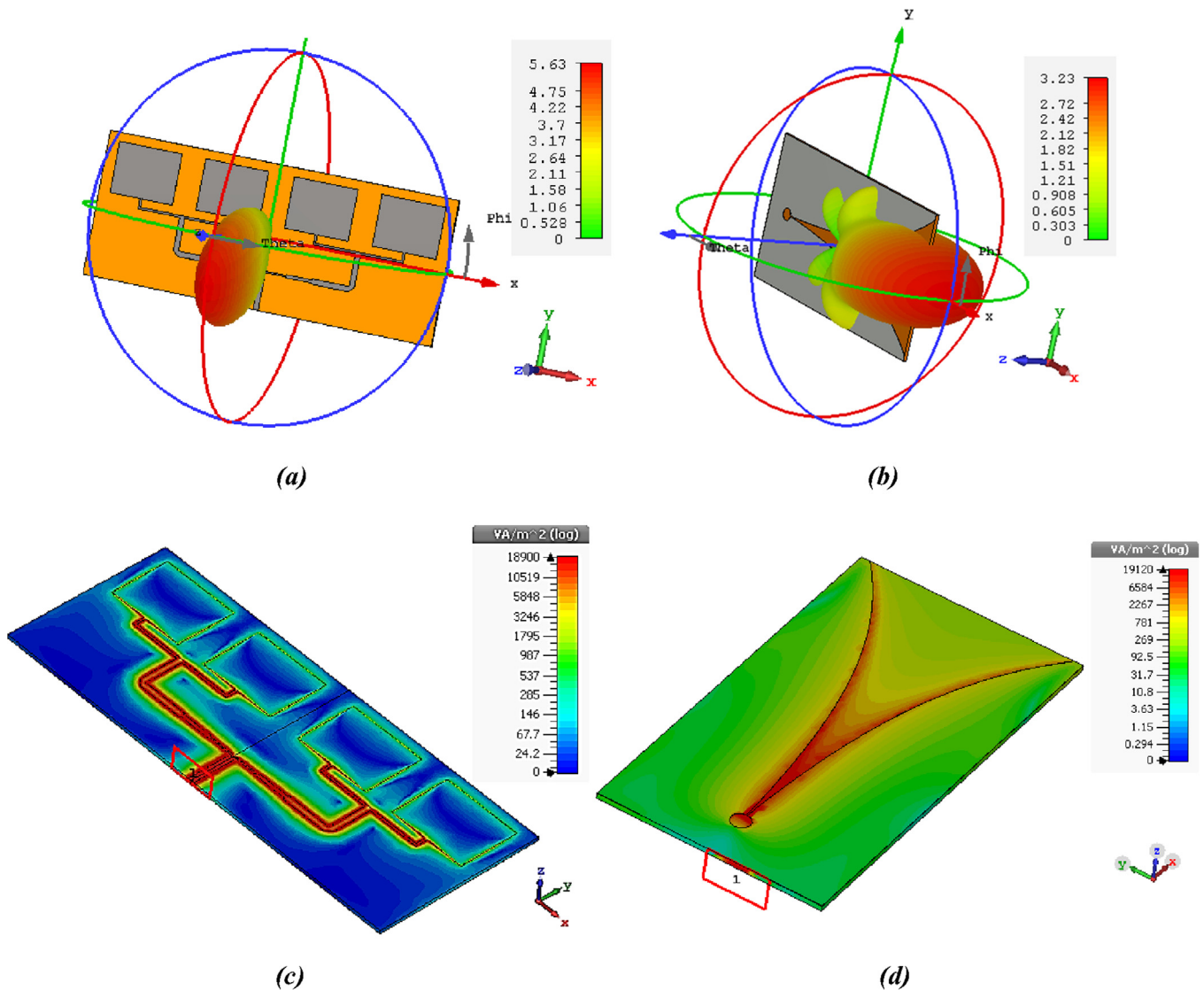

Fig. 4. Simulation and measurement results of far-field of the antennas. (a) Far-field results of Rx array antenna in elevation pattern ($\varphi = 0$). (b) Far-field results of Tx Vivaldi antenna in elevation pattern ($\varphi = 0$).

Fig. 5. 3D simulation results of the antennas. (a) Gain pattern of the receiver antenna in linear scaling (b) Gain pattern of the transmitter antenna in linear scaling (c) Power flow of the receiver antenna in log scaling (d) Power flow of the transmitter antenna in log scaling.

additionally concluded from the power pattern that dielectric loss mechanism in the substrate plays a more significant role for the transmitter antenna. The loss tangent of FR-4 substrate used in the simulations is $\tan\delta = 0.025$. Fig. 5 shows the expected symmetric behaviour of the fields in the far-field region. The power distributions on the surface of the structures without any abnormal fluctuations at the edges or on the structures.

5. Unequal power divider implementation

An unequal power divider is designed, realized and integrated to the Doppler radar in order to transmit a higher power to the Tx as compare to the mixer. The dividing ratio for the proposed power splitter is adjusted as ~1:3 instead of 1:1 (equal dividing) in order to improve maximum range of the radar. Increase in the range is estimated according to a transmission experiment performed in an anechoic chamber by using a signal source, our transmitter and receiver antennas, a spectrum analyser, an equal and an unequal power divider. In the first case, an equal power divider is used between the signal generator and the Tx such that received power at the Rx is measured to be −15.17 dBm. The second experiment is repeated for an unequal power divider where the signal level at

the Rx is observed to be −13.00 dBm. The range improvement is calculated as ~12% from the radar range equation in the case of using unequal power splitter in the system according to the increase in the received power at Rx for the given parameters of antennas, distance between two antennas and the operating wavelength.

In Fig. 6a, the comparison of the transmission parameters is illustrated. The equal power divider has −4 dB insertion loss while the high power port of the unequal power divider has −2 dB insertion loss. We assume that the reason of fluctuations in the measurement results is in the lack of high accuracy in our VNA measurements. In Fig. 6b, the power flow of the unequal power divider can be seen. As it is expected, more power is rotated to the wider line while the narrower line transmits less power. The shape of the unequal power divider and the critical parameters for the design of T-Junction power divider are given in Fig. 6c and Table 3 where the thickness of the FR-4 substrate is 1.5 mm.

6. Integration of the antennas to the Doppler radar and experimental results

In MIT Coffee Can Radar [8–16], a 2.45 GHz continuous wave signal is generated by a solid state oscillator and it is split into
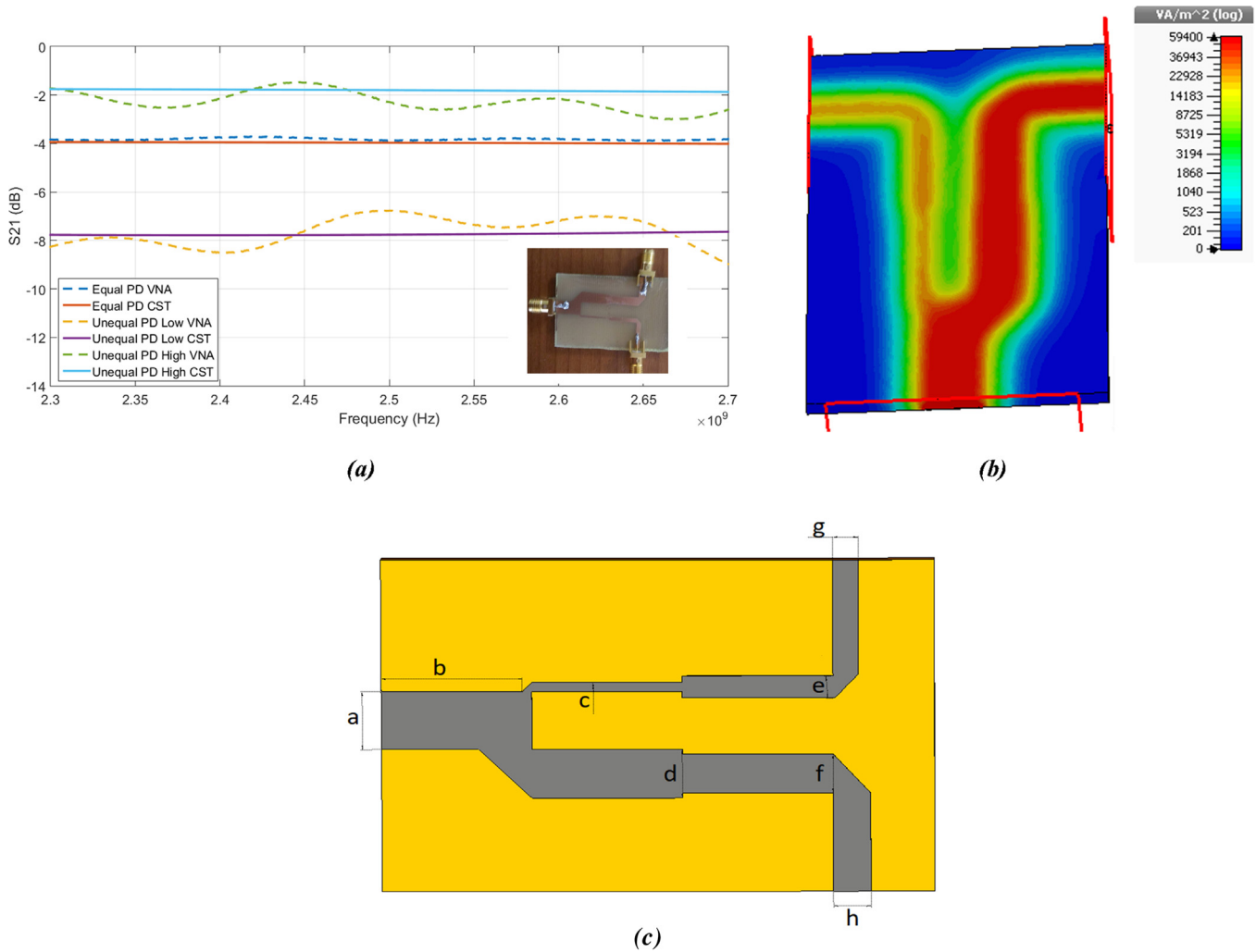
(a)

(b)

(c)

Fig. 6. Power Divider. (a) S21 comparison for the power dividers. (b) Power flow simulation of an unequal power divider. (c) Shape of the unequal power divider.

Table 3
Dimensions for the Unequal Power Divider.

Parameter	a	b	c	d	e	f	g	h
Value (mm)	4.96	11.05	0.75	4.18	1.86	3.34	2.00	2.94

two parts such that the first part is transmitted to the free space and the other one is used at the mixer to obtain a signal which oscillates with the frequency shift (Doppler frequency) in the received signal. The output signal of the mixer is transmitted to a computer via microphone cable and the data is recorded as a single sound file. Afterwards, open source software [10] is used to process the input information for finding velocity and related parameters.

Initial design of Doppler radar at IZTECH Lab. [11] was operating at 2.60 GHz according to the mentioned principles. The system used two-element array for the receiver and a single patch antenna for the transmitter, [33,34]. However, main characteristics, e.g. radiation pattern, half power beamwidth, gain, directivity of these antennas were insufficient for mechanical angular scanning. Additionally, the radar operating frequency was not in the ISM band according to ITU-Radio Regulations. Later on the possibility of using cantennas in scanning was examined, [35]. The mechanical and beamwidth issues showed that new concepts are needed for both antennas. The study [36], achieved the desired antenna parameters necessary at 2.45 GHz for the considered

application. For instance, a much narrower beamwidth is obtained for the receiver and antenna gains are increased as compare to [19] to have a larger range and target recognition sensitivity. Furthermore, the current study, which is based on [36,37] contains novelties in antenna designs and can be considered as a *proof of concept* work for angular scanning operation on MIT Doppler Radar system.

Antennas are considered to be located on the same platform. Due to the possibility of an undesired mutual coupling the convenience of the distance between the transmitter and receiver was checked before the integration. The case is tested via simulation see Fig. 7a such that obtained results are consistent with measurements. The structure is modelled as a two port network. Antennas are connected to each port at certain orientations according to radiation patterns. The coupled power is found as 0.003 and 0.002 percent of the input power from the S12 and S21 values, respectively. Therefore, the distance between antennas is considered to be sufficient at this frequency for the efficient operation of the radar. The antennas mounted to system are shown in Fig. 7b.
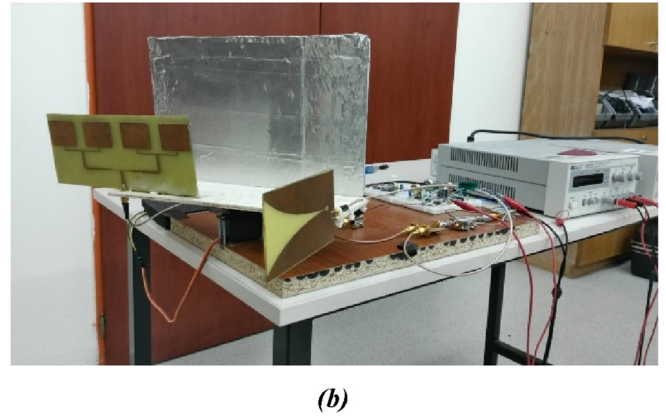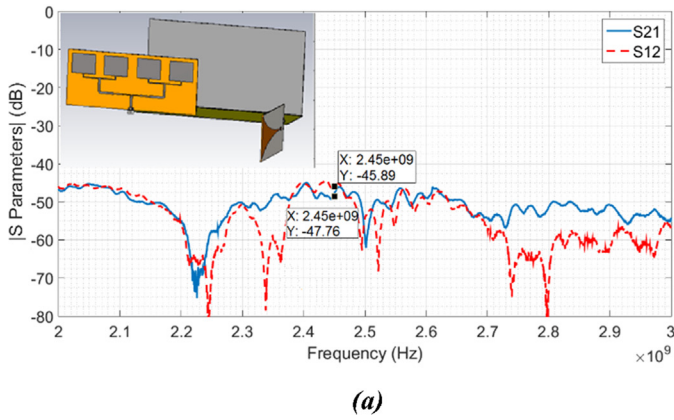
Fig. 7. System integration of the antennas. (a) S_{21} and S_{12} results of the antennas. (b) The operational view of the fabricated antennas on the radar.

At this point, we express the operation principle of the newly adapted angular scanning feature and illustrate interesting results in the following figures. In tracking mode, antennas are rotated clockwise/counter-clockwise between 18°-162° with 36° angular steps via a servo motor which carries a thin wooden plate holding Tx - Rx and a conducting plate reflector. In each time step (indicated as 'Step' in figures), a certain section/pie slice in the radar range is scanned for 1 s, then the motor turns and the listening section is updated accordingly. For instance, the radar is listening sector 2 angles: 54–90° at a given time in Fig. 8, such that the observed area is indicated as a green bordered region in the polar plot. The received signal is processed and the results are shown immediately as a velocity–step–normalized power plots. The first of the 5 subplots in Fig. 8 is concerned with the entire Doppler signal which evolves in time until the radar operation is terminated. The other 4 subplots belonging to each of the 4 sections, e.g. the second subplot represents the 1st section between 18° and 54°, and the third subplot indicates the 2nd section between 54° and 90°, and so forth.

The velocity plot of the Fig. 8 expresses the uninterrupted movements of a target in a particular area, we call the 4th section defined by the angles, {126° − 162°}. In this experiment an average size human is walking with a speed of less than ∼3 m/s such that radar scans this section 3 times during its total scan run, see the following subplot in Fig. 8 entitled with the velocity for entire Doppler signal. On the other hand, since there are no moving objects in the other sections, which are blind sectors, the related subplots are dark blue coloured. This simple experiment shows that finer angular location can be obtained if the antenna footprint and the angular scanning step are reduced for the prototype radar. However, 30° beamwidth with 36° scanning step is used for scanning due to the trade-off between the size of the Rx and the 3 dB beamwidth.

Fig. 9 is basically related to the line of sight (LOS) and through wall imaging (TWI) cases. The experiment result which can be followed in Fig. 9a is for two targets moving in the 2nd and 4th sections. The power variations on the plots indicate whether the target moves away from the radar. Conversely the signal level increases when the distance between target and radar decreases,
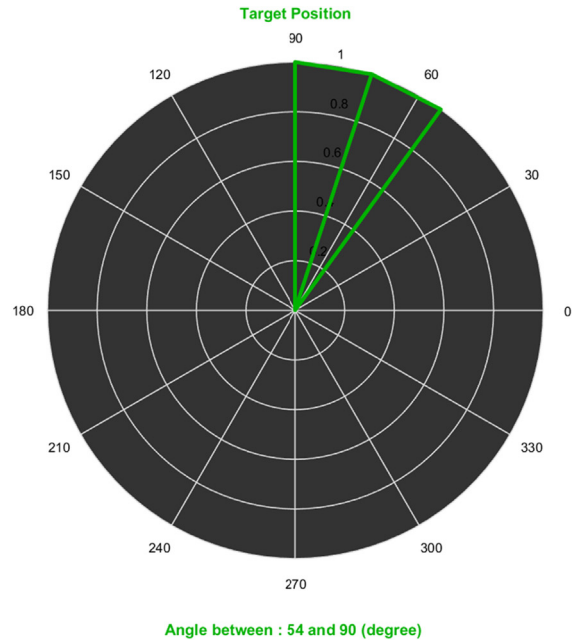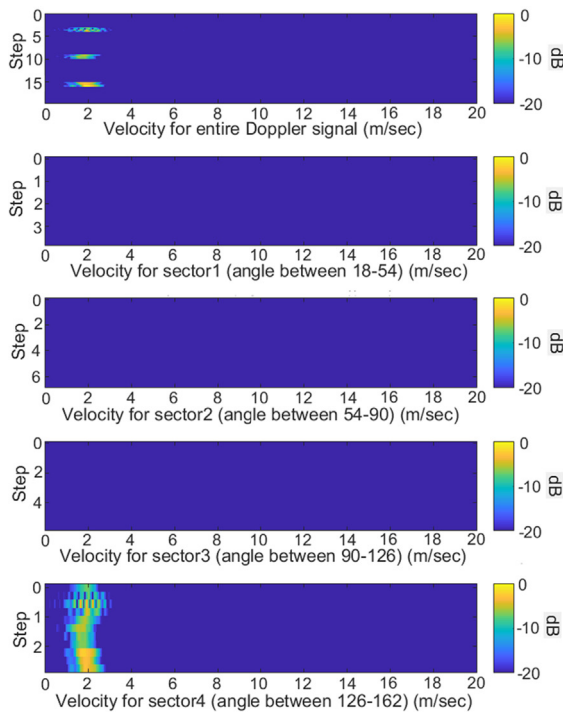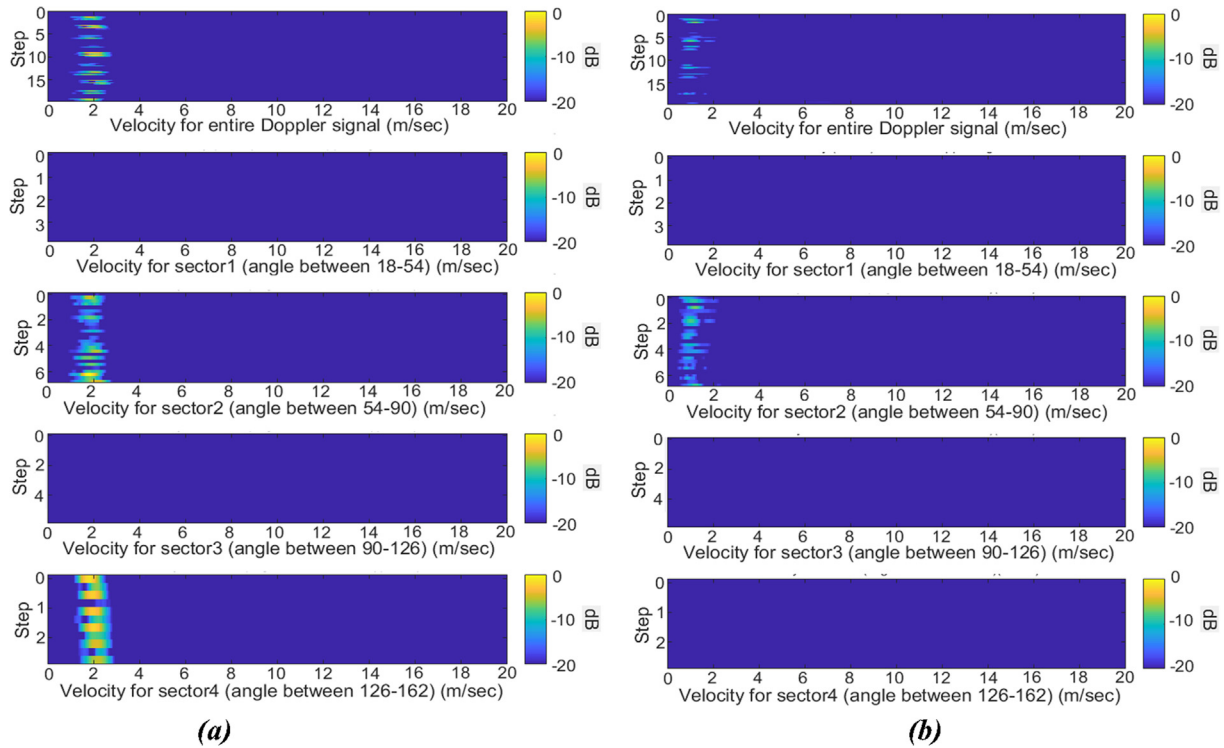

Fig. 8. Improved interface for angular scanning.

Fig. 9. Velocity measurement and sector classification. (a) Measurements via angular scanning LOS application. (b) Measurements via angular scanning TWI application.

see the changes in Fig. 9a, the subplot entitled velocity for sector 2 (angle between 54 and 90). Although the human walking targets at the 2nd and 4th sections are uninterrupted, the subplots of 1st and 3rd sections are dark blue since the footprint of the radar is delimitated by the receiver antenna, appropriately. Fig. 9b refers to the TWI case for a target moves only in the 2nd sector. In this scenario, a moving target behind a ~20 cm thick standard concrete wall walks away from the radar such that the traces in the radar are faded. Periodically clockwise and counter-clockwise rotating radar antennas do not sense any movement except for the related 2nd section similar to the former experiments.

Fig. 10 illustrates radar traces when an average size human walks and runs in the 3rd section for two different scenarios. The total radar operation takes ~16 s where the first figure is devoted for LOS case and the second figure is prepared for TWI application. The result for TWI is obtained when the radar is 1 m away from

concrete wall and the target is approximately 5 m behind the wall during the angular scanning.

It can be concluded from Figs. 9, 10 that the radar can classify the type of movement, indicate and quantify the speed increase for the running action even in the case of a concrete wall between the radar and the target. Furthermore, the targets through the wall can be observed with the microstrip antennas, see Fig. 10b, which
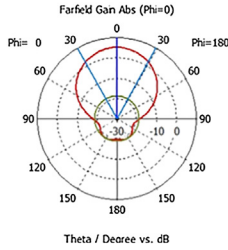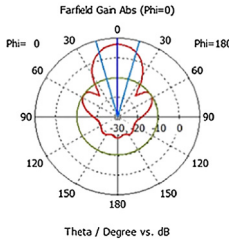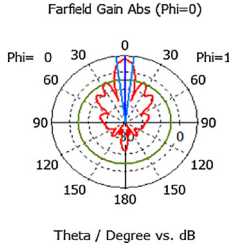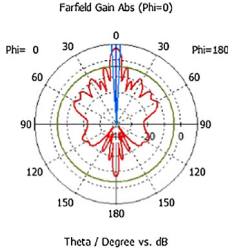
Table 4
Comparison between the radars in terms of the angular scanning capability.

Parameter	Proposed Radar	Ref-1	Ref-2
Footprint	~35 deg	~75 deg	~60 deg
Back-lobe Level	−18 dB	−12 dB	−17 dB
Weight of the antennas	60 gr	350 gr	35 gr
Mutual Coupling	−45 dB	−30 dB	−35 dB
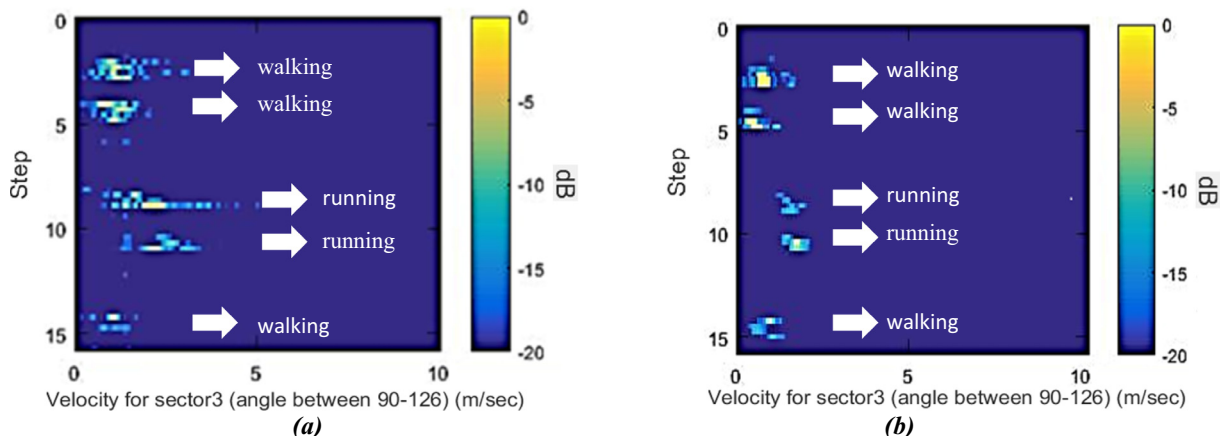
Fig. 10. Velocity measurement and action classifications. (a) Measurements via angular scanning LOS application. (b) Measurements via angular scanning TWI application.

Table 5
Effects of number of antenna elements on the antenna design parameters.

Parameter	Number of Elements: 2	Number of Elements: 4	Number of Elements: 8	Number of Elements:16
Width of the Antenna (mm)	110	220	440	880
Z_{in} (ohm)	53.5	50.8	49.1	47.6
Main Lobe Magnitude (dB)	5.05	6.90	7.41	7.58
Side-lobe level (dB)	−23.9	−17.5	−12.0	−11.3
3-dB beamwidth (degree)	59	31	14	7
Farfield Gain Pattern				

was recently reported for a horn antenna in [17]. According to the LOS experiments, the maximum distance where the received power is separable from the background noise is approximately 20 m in the laboratory conditions while the walking man carries a square metal reflector plate having one edge 50 cm. Otherwise, the radar range is ∼16 m.

In Table 4, angular scanning capability of the proposed radar is compared for different antenna mounts. Here, the radar having cantennas is called as Ref-1 [10], and the radar with a 2 × 1 patch array antenna is indicated as Ref-2, [33]. In this table, footprint indicates the angle that radar can scan at each step. The undesired power leak which can be localized behind of the antenna is presented by the Back-lobe level. Mutual coupling describes the coupling magnitude (S_{21}) between the transmitter and the receiver antennas. Weight of the antennas indicates the total weight of both Tx and Rx.

Antennas of the proposed radar have the minimum mutual coupling and the smallest footprint for the receiver according to results given in Table 4. Both of these parameters are crucial for the desired angular scanning application. The mutual coupling is related to the locations of the Tx/Rx antennas on the same platform and hence to the compactness of the system, and the small beamwidth provides a more precise angular location of the target. Note that the smaller footprint is achievable with larger number of microstrip array elements, see Appendix A, which makes the system inappropriate for the selected application. Hence the design concept of the receiver antenna should be change for the narrower beamwidth. The weight of the proposed antennas ∼6 times lighter and are less bulky as compare to the original design Ref-1, and they have the smallest magnitude of back-lobe level.

7. Conclusion

In this study, experiences and findings on the design, simulation, measurements and integrations of the patch array and Vivaldi types of microstrip antennas with a mechanical angular scan feature for the MIT Coffee Can Radar is reported. The range of the radar is improved with the adaptation of an unequal power divider to the radar. Furthermore, experimental results are illustrated by using the updated compact prototype of the radar for the cases of multi-target tracking in different angular sections, movement classifications and through wall identifications.

The necessary antenna design criteria are met for such an application at the operating frequency 2.45 GHz. Experimental results show that the radar can identify the moving target locations at certain sections depending on beamwidth of the receiver antenna and the step size of the scanning angle. It is shown that through wall

target sensing is achievable with the proposed microstrip antennas which are lighter as compare to horn antennas. Furthermore, it is illustrated that more accurate angular location identifications are possible via larger amount of array elements in the receiver with corresponding smaller angular sweeping steps in rotation. As a future study, the current prototype will be extended to a higher range and resolution performance for more complicated scenarios via mechanical, software and hardware updates.

Acknowledgments

Appendix A

See Table 5.

References

[1] Rabbani MS, Ghafouri-Shiraz H. Accurate remote vital sign monitoring with 10 GHz ultra-wide patch antenna array. Int J Electron Commun (AEÜ) 2017;77:36–42.

[2] Li C, Ling J, Li J, Lin J. Accurate Doppler radar noncontact vital sign detection using the RELAX algorithm. IEEE Trans Instrument Measure 2010;59(3).

[3] Gao H, Xie L, Wen S, Kuang Y. Micro-Doppler signature extraction from ballistic target with micro-motions. IEEE Trans AES 2010;46(4):1968–82.

[4] Biebl EM. RF systems based on active integrated antennas. Int J Electron Commun (AEÜ) 2003;57(3):173–80.

[5] Stabile TA, Perrone A, Gallipoli MR, Ditommaso R, Ponzo FC. Dynamic survey of the Musmeci bridge by joint application of ground-based microwave radar interferometry and ambient noise standard spectral ratio techniques. IEEE Geosci Remote Sens Lett 2013;10(4).

[6] Yeary M, Cheong BL, Kurdzo JM, Yu TY, Palmer R. A brief overview of weather radar technologies and instrumentation. IEEE Instrum Meas Mag 2014. pp. 1094-6969/14/©2014IEEE 2014.

[7] Lavery MPJ, Speirits FC, Barnett SM, Padgett MJ. Detection of a spinning object using light's orbital angular momentum. Science 2013;341(6145):537–40. https://doi.org/10.1126/science.1239936.

[8] Gürbüz SZ, Özcan MB, Parım AB, et al. Target detection and ranging with the 2.4 GHz MIT coffee can radar. In: IEEE 22nd Signal Processing and Communication Applications Conference, Trabzon, Turkey; April 2014. p. 1450–53.

[9] Jensen MA, Arnold DV, Crockett DE. System-level microwave design: radar based laboratory project. IEEE Trans Educ 2000;43(4):414–9.

[10] MIT OpenCourseWare: Build a small radar system capable of sensing range, doppler, and synthetic aperture radar imaging', https://ocw.mit.edu [accessed May 2017].

[11] Kabukçu YU, Çelik S, Salan O, et al. FMCW Doppler radar measurements with microstrip tx-rx antennas. In: Abstract for the ICRST 2016 18th International Conference on Radar Science and Technology, Barcelona, Spain; August 2016.

[12] Abbasi HA, Shaukat SH, Shaheen I, et al. Cost effective FMCW radar for Doppler and ranging. Int J Comput Sci Softw Eng (IJCSSE) 2015;4(6):137–40.

[13] Basarslan O, Yaldiz E. Implementation of FMCW radar for training applications. In: 4th International Conference on Electrical and Electronics Engineering, Ankara, Turkey. p. 304–8.

[14] Schneider D. Coffee-can radar: How to build a synthetic aperture imaging system with tin cans and AA batteries. IEEE Spectr 2012;49(11):24–5.

[15] Carroll J, Paparisto G, Vye D. The "coffee-can" radar redesigned as an inexpensive RF PCB. IEEE Microwave Mag 2016;17(10):62–74.

[16] Charvat GL. Small and Short Range Radar Systems. 1st ed. Boca Raton: CRC Press; 2014.

[17] Gennarelli G, Ludeno G, Soldovieri F. Real-time through-wall situation awareness using a microwave Doppler radar sensor. Remote Sens. 2016;8:621.

[18] Skolnik MI. Introduction to Radar Systems. 3rd ed. New Delhi: Tata McGraw Publishing; 1962 (1981).

[19] Balanis CA. Antenna Theory: Analysis and Design. 3rd ed. Hoboken: Wiley; 1982 (2005).

[20] Pozar DM. Microwave Engineering. 4th ed. New York: Wiley; 1990 (2012).

[21] Aye ET, Nwe CM. Rectangular microstrip patch antenna array for RFID application using 2.45 GHz frequency range. Int J Sci Res Pub 2014;4(6):1–7.

[22] Khraisat YSH. Design of 4 elements rectangular microstrip patch antenna with high gain for 2.4 GHz Applications. Modern Appl Sci 2012;6(1):68–74.

[23] Wahab NA, Maslan ZB, Muhamad WMW, et al. Microstrip Rectangular 4x1 patch array antenna at 2.5 GHz for a WiMax application. In: WiMax application' 2nd International Conference on Computational Intelligence, Communication Systems and Networks, Liverpool, UK, July. p. 164–8.

[24] Patil SM, Bombale UL. Design analysis and study of 2x1 rectangular microstrip antenna array at 2.45 GHz for beam steering. Int J Eng Res Appl 2013;3 (1):1242–5.

[25] Alsageri AF. Design and analysis of microstrip patch antenna arrays', MSc thesis. University College of Borås; 2011.

[26] Pandey GK, Singh HS, Bharti PK, et al. High gain Vivaldi antenna for radar and microwave imaging applications. Int J Sig Proc Sys 2015;3(1):35–9.

[27] Herzi R, Zairi H, Gharsallah A. Reconfigurable Vivaldi antenna with improved gain for uwb applications. Microwave Opt Technol Lett 2016;58(2):490–4.

[28] Fang G, Sato M. Optimization of Vivaldi antenna for demining by GPR. In: Interim International Symposium on Antennas and Propagation, Yokosuka, Japan; November 2002. p. 263–66.

[29] Yang Y, Wang Y, Fathy AE. Design of compact Vivaldi antenna arrays for UWB see through wall applications. Progr Electromag Res 2008;82:401–18.

[30] Bozdağ G. Novel microstrip antennas for multiband and wideband applications. MSc thesis. Izmir Institute of Technology; 2014.

[31] Bhartia P, Bahl I, Garg R, et al. Microstrip Antenna Design Handbook. 1st ed. Nordwood: Artech House Publishers; 2001 (2001).

[32] James JR, Hall PS, Wood C. Microstrip Antenna Theory and Design. London: IEE Electromagnetic Waves Series, Peter Peregrinus Ltd; 1981.

[33] Altuntas M. Design and implementation of microstrip antenna for FMCW Doppler radar BSc project. Izmir Institute of Technology; 2014.

[34] Celik S, Salan O. Doppler radar design BSc project. Izmir Institute of Technology; 2015.

[35] Kethuda O. System experiments, simulations and integrations of Cantennas to the Doppler radar BSc project. Izmir Institute of Technology; 2016.

[36] Karatay A. Design, implementation and integration of Tx/Rx microstrip antennas for a Doppler radar BSc project. Izmir Institute of Technology; 2017.

[37] Orcan D, Ozkal C. Implementations of angular identification mechanisms for a doppler radar BSc project. Izmir Institute of Technology; 2017.